INTERNATIONAL JOURNAL FOR NUMERICAL METHODS IN FLUIDS
Int. J. Numer. Meth. Fluids 2001; **37**: 23–43 (DOI: 10.1002/fld.162)

Numerical simulation of the vertical structure of discontinuous flows

Guus S. Stelling[a,b,*,1] and Marcela M. Busnelli[b]

[a] *Delft Hydraulics, Delft, Netherlands*
[b] *Faculty of Civil Engineering, Delft University of Technology, Delft, Netherlands*

SUMMARY

A numerical method to solve the Reynolds-averaged Navier–Stokes equations with the presence of discontinuities is outlined and discussed. The pressure is decomposed into the sum of a hydrostatic component and a hydrodynamic component. The numerical technique is based upon the classical staggered grids and semi-implicit finite difference methods applied for quasi- and non-hydrostatic flows. The advection terms in the momentum equations are approximated in order to conserve mass and momentum following the principles recently developed for the numerical simulation of shallow water flows with large gradients. Conservation of these properties is the most important aspect to represent near local discontinuities in the solution, following from sharp bottom gradients or hydraulic jumps. The model is applied to reproduce the flow over a step where a hydraulic jump forms downstream. The hydrostatic pressure assumption fails to represent this type of flow mainly because of the pressure deviation from the hydrostatic values downstream the step. Fairly accurate results are obtained from the numerical model compared with experimental data. Deviation from the data is found to be inherent to the standard k–ε model implemented. Copyright © 2001 John Wiley & Sons, Ltd.

KEY WORDS: advection approximations; discontinuous flows; non-hydrostatic free surface flows; staggered grids

1. INTRODUCTION

For shallow water flow problems with hydraulic jumps, the so-called 'Godunov methods' developed for aerodynamics are applied [1–3]. Recently, a numerical method for shallow water flows with large gradients has been outlined by Stelling *et al.* [4], which is based upon the classical staggered grids and implicit integration schemes, such as those described by Leendertse [5] and Casulli [6]. The continuity equation is approximated in such a fashion that mass

* Correspondence to: Delft Hydraulics, PO Box 177, 2600 MH Delft, Netherlands. Tel.: +31 15 2858762/2781953.
[1] E-mail: Guus.Stelling@wldelft.nl

Received November 1999
Revised August 2000

is conserved not only globally but also locally. The momentum equation is approximated to fulfil a proper momentum balance near large gradients.

This paper describes how the numerical principles described by Stelling *et al.* [4] are extended to the full Reynolds-averaged Navier–Stokes equations for simulating non-hydrostatic flows with steep gradients. A semi-implicit finite difference method for non-hydrostatic flows, recently developed by Casulli and Stelling [7], is applied to solve the equations. The technique is based upon a fractional step method, where the hydrostatic and the hydrodynamic components of the pressure are considered separately. The mass conservation assures a stable numerical solution; a proper momentum balance provides that this stable solution converges. The resulting algorithm is relatively simple and numerically stable even at large Courant numbers.

2. GOVERNING EQUATIONS

The governing equations are the Navier–Stokes equations for incompressible fluid which expressed in two dimensions are

Momentum equations:

$$\frac{\partial u}{\partial t}+u\frac{\partial u}{\partial x}+w\frac{\partial u}{\partial z}=-\frac{\partial p}{\partial x}+\nu_{\mathrm{h}}\frac{\partial^2 u}{\partial x^2}+\frac{\partial}{\partial z}\left(\nu_{\mathrm{t}}\frac{\partial u}{\partial z}\right) \tag{1}$$

$$\frac{\partial w}{\partial t}+u\frac{\partial w}{\partial x}+w\frac{\partial w}{\partial z}=-\frac{\partial p}{\partial z}+\nu_{\mathrm{h}}\frac{\partial^2 w}{\partial x^2}+\frac{\partial}{\partial z}\left(\nu_{\mathrm{t}}\frac{\partial w}{\partial z}\right)-g \tag{2}$$

Continuity equation:

$$\frac{\partial u}{\partial x}+\frac{\partial w}{\partial z}=0 \tag{3}$$

where $u(x, z, t)$ and $w(x, z, t)$ are the velocity components in the horizontal x- and vertical z-direction respectively, t is the time; $p(x, z, t)$ is the normalized pressure defined as the pressure divided by a constant reference density; g is the gravitational acceleration and ν_{h} and ν_{t} are the horizontal and vertical turbulence viscosity respectively.

Integrating Equation (3) over the depth and using a kinematic condition at the free-surface leads to the following free-surface equation:

$$\frac{\partial \zeta}{\partial t}+\frac{\partial}{\partial x}\left[\int_{-h}^{\zeta} u\,\mathrm{d}z\right]=0 \tag{4}$$

where $\zeta(x, t)$ is the free-surface level above the reference plane and $h(x)$ is the water depth measured from the undisturbed water surface (Figure 1).

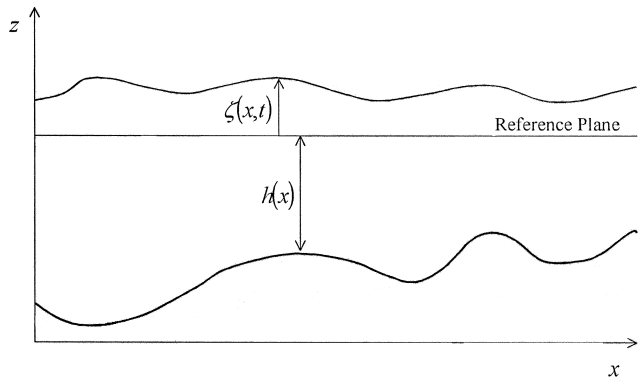

Figure 1. Flow schematization.

The pressure $p(x, z, t)$ in Equations (1) and (2) can be decomposed into the sum of its hydrostatic and non-hydrostatic components. The hydrostatic pressure component is determined from the vertical momentum equation (2) by neglecting the convective and the viscous acceleration terms. This gives

$$p(x, z, t) = g[\zeta(x, t) - z] + q(x, z, t) \tag{5}$$

where $q(x, z, t)$ denotes the non-hydrostatic or the hydrodynamic pressure component. By substituting Equation (5) in Equations (1) and (2) the following equations are obtained:

$$\frac{\partial u}{\partial t} + u\frac{\partial u}{\partial x} + w\frac{\partial u}{\partial z} = -g\frac{\partial \zeta}{\partial x} - \frac{\partial q}{\partial x} + \nu_h\frac{\partial^2 u}{\partial x^2} + \frac{\partial}{\partial z}\left(\nu_t\frac{\partial u}{\partial z}\right) \tag{6}$$

$$\frac{\partial w}{\partial t} + u\frac{\partial w}{\partial x} + w\frac{\partial w}{\partial z} = -\frac{\partial q}{\partial z} + \nu_h\frac{\partial^2 w}{\partial x^2} + \frac{\partial}{\partial z}\left(\nu_t\frac{\partial w}{\partial z}\right) \tag{7}$$

3. NUMERICAL APPROXIMATION

The numerical method described by Casulli and Stelling [7] to solve Equations (4), (6) and (7) is applied. The momentum equations are split and free-surface elevation and hydrodynamic pressures are determined in two steps. First, the hydrodynamic pressure is assumed null and free-surface levels are obtained from Equations (4) and (6). When the hydrostatic approximation is made, $q(x, z, t) = 0$ is assumed throughout. In this step, the non-hydrostatic component of the pressure is assumed not to have an effect on the resulting flow. In the second step the velocities are corrected by considering the hydrodynamic pressure terms.

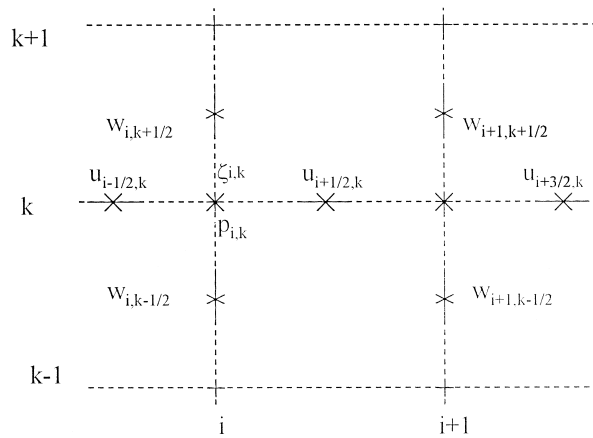

Figure 2. Control volume.

For the numerical application a fully staggered grid is applied, a so-called C grid. Water levels and pressures are approximated at locations (i, k), horizontal velocities at $(i+1/2, k)$ and vertical velocities at $(i, k+1/2)$ (Figure 2).

3.1. First step: hydrostatic pressure

The first step is performed by neglecting the contribution of the hydrodynamic pressures. The resulting velocity field and water surface elevation at the new time step are not yet final and will be denoted by u^* and w^* respectively. A semi-implicit discretization for the momentum equations (6) and (7) takes the following form:

$$u^*_{i+1/2,k} = u^n_{i+1/2,k} - \Delta t\,\mathrm{ADV}(u^n_{i+1/2,k}) + \Delta t\,\mathrm{HV}(u^n_{i+1/2,k}) - (1-\theta)\frac{\Delta t}{\Delta x}\left[g(\zeta^n_{i+1} - \zeta^n_i)\right] - \theta g \frac{\Delta t}{\Delta x}(\zeta^{n+1}_{i+1} - \zeta^{n+1}_i) + \nu_t \Delta t \frac{\dfrac{u^*_{i+1/2,k+1} - u^*_{i+1/2,k}}{\Delta z^n_{i+1/2,k+1/2}} - \dfrac{u^*_{i+1/2,k} - u^*_{i+1/2,k-1}}{\Delta z^n_{i+1/2,k-1/2}}}{\Delta z^n_{i+1/2,k}} \tag{8}$$

$$w^*_{i,k+1/2} = w^n_{i,k+1/2} - \Delta t\,\mathrm{ADV}(w^n_{i,k+1/2}) + \Delta t\,\mathrm{HV}(w^n_{i+k+1/2}) + \nu_t \Delta t \frac{\dfrac{w^*_{i,k+3/2} - w^*_{i,k+1/2}}{\Delta z^n_{i,k+1}} - \dfrac{w^*_{i,k+1/2} - w^*_{i,k-1/2}}{\Delta z^n_{i,k-1}}}{\Delta z^n_{i,k+1/2}} \tag{9}$$

In Equations (8) and (9) ADV and HV are finite difference operators that include the explicit discretization of the advection terms and horizontal viscosity terms respectively.

Equation (9) forms a linear tridiagonal system with unknowns w^* on the same water column. The provisional vertical component of the velocity can be obtained by the double sweep algorithm. Equation (8) also constitutes a linear tridiagonal system, which, however, is coupled to the unknown water surface elevation ζ^{n+1}. In order to determine ζ^{n+1}, the discretized continuity equation (4) is required

$$\zeta_i^{n+1} = \zeta_i^n - \frac{\Delta t}{\Delta x}\theta\left[\sum_{k=m}^{M} \Delta z_{i+1/2,k}^n u_{i+1/2,k}^* - \sum_{k=m}^{M} \Delta z_{i-1/2,k}^n u_{i-1/2,k}^*\right] - \frac{\Delta t}{\Delta x}(1-\theta)\left[\sum_{k=m}^{M} \Delta z_{i+1/2,k}^n u_{i+1/2,k}^n - \sum_{k=m}^{M} \Delta z_{i-1/2,k}^n u_{i-1/2,k}^n\right] \tag{10}$$

Velocities from Equation (8) are substituted into Equation (10). The resulting equation constitutes a tridiagonal system with the free-surface elevation as unknown. The system is solved by the double sweep algorithm. Boundaries upstream and downstream are defined. Any assumption of the initial free-surface elevation should be valid as long as it leads to positive water depths. In the simulation included in this article, the initial water level is assumed constant all over the reach and equal to the downstream boundary. Discharge is prescribed at the upstream boundary. Downstream, a constant water surface level is imposed. Once the new free-surface levels are computed, the horizontal velocities u^* are obtained from Equation (8). The boundary condition at the bed is given by the logarithmic law of the wall as (see Rodi [8])

$$\nu_t \frac{\partial u}{\partial z} = u^{n+1} \frac{|u^n|}{\left(\frac{\sqrt{g}}{\kappa}\ln\left(1+\frac{0.5\Delta z}{z_0}\right)\right)^2} \tag{11}$$

where κ is the von Karman constant and z_0 is the friction parameter.

3.2. Second step: non-hydrostatic pressure correction

In the second step the new velocity fields u^{n+1} and w^{n+1} are computed by including the hydrodynamic pressures terms into the momentum equation. In this way the provisional velocity field is corrected by considering the non-hydrostatic pressures.

The discrete momentum equations are

$$u_{i+1/2,k}^{n+1} = u_{i+1/2,k}^* - \frac{\Delta t}{\Delta x}(q_{i+1,k}^{n+1} - q_{i,k}^{n+1}) \tag{12}$$

$$w_{i,k+1/2}^{n+1} = w_{i,k+1/2}^* - \frac{\Delta t}{\Delta z_{i,k+1/2}^n}(q_{i,k+1}^{n+1} - q_{i,k}^{n+1}) \tag{13}$$

Cells below the free-surface should verify the discretized incompressibility condition (Equation (3))

$$\frac{u_{i+1/2,k}^{n+1}\Delta z_{i+1/2,k}^n - u_{i-1/2,k}^{n+1}\Delta z_{i-1/2,k}^n}{\Delta x} + w_{i,k+1/2}^{n+1} - w_{i,k-1/2}^{n+1} = 0 \tag{14}$$

An equation for the non-hydrostatic pressure $q_{i,k}^{n+1}$ under the free surface is derived by substituting the expressions for the new velocities from Equations (12) and (13) into Equation (14). The following finite difference equation is obtained:

$$\Delta t \frac{(q_{i+1,k}^{n+1} - q_{i,k}^{n+1})\Delta z_{i+1/2,k}^{n} - (q_{i,k}^{n+1} - q_{i-1,k}^{n+1})\Delta z_{i-1/2,k}^{n}}{\Delta x^2} + \Delta t \frac{(q_{i,k+1}^{n+1} - q_{i,k}^{n+1})}{\Delta z_{i,k+1/2}^{n}}$$
$$- \Delta t \frac{(q_{i,k}^{n+1} - q_{i,k-1}^{n+1})}{\Delta z_{i,k-1/2}^{n}} = \frac{u_{i+1/2,k}^{*}\Delta z_{i+1/2,k}^{n} - u_{i-1/2,k}^{*}\Delta z_{i-1/2,k}^{n}}{\Delta x} + w_{i,k+1/2}^{*} - w_{i,k-1/2}^{*} \tag{15}$$

Equation (15) forms a five diagonal linear system, which is solved by the preconditioned conjugate gradient method.

Once the non-hydrostatic pressure is computed, the corresponding horizontal velocity field is obtained from Equation (12), while the vertical component of the velocity can be obtained, equivalently, either from Equation (13) or from the continuity equation (14).

4. ADVECTION APPROXIMATION

For numerical approximations, conservation of properties is important near large local gradients. Near steep bottom gradients, mass conservation seems to be imperative.

The advection terms in the momentum equations are approximated in order to conserve mass and momentum following the same principles described by Stelling *et al.* [4] for shallow water flows.

4.1. Momentum equation in the horizontal direction

The continuity equation is discretized as follows:

$$\frac{\bar{u}_{+} - \bar{u}_{-}}{\Delta x} + \frac{\bar{w}_{+} - \bar{w}_{-}}{\Delta z} = 0 \quad \text{at } (i,k) \tag{16}$$

The momentum equation is approximated for positive flows as follows:

$$\frac{\partial u}{\partial t} + \bar{u}_{-}\left(\frac{u - u_{-1,}}{\Delta x}\right) + \bar{w}_{-}\left(\frac{u - u_{,-1}}{\Delta z}\right) = -g\frac{\partial \zeta}{\partial x} - \frac{\partial q}{\partial x} + \nu_{\mathrm{h}}\frac{\partial^2 u}{\partial x^2} + \frac{\partial}{\partial z}\left(\nu_{\mathrm{t}}\frac{\partial u}{\partial z}\right)$$
$$\text{at } (i+1/2,k) \tag{17}$$

where

$$\bar{u}_{+} = \frac{u_{i+1/2,k} + u_{i+3/2,k}}{2}$$

$$\bar{u}_{-} = \frac{u_{i-1/2,k} + u_{i+1/2,k}}{2}$$

$$\bar{w}_{+} = \frac{w_{i,k+1/2} + w_{i+1,k+1/2}}{2} \tag{18}$$

$$\bar{w}_{-} = \frac{w_{i,k-1/2} + w_{i+1,k-1/2}}{2}$$

$$u_{-1,} = u_{i-1/2,k}$$

$$u_{,-1} = u_{i+1/2,k-1}$$

The fact that Equation (17) describes a momentum balance can be demonstrated by rewriting Equation (17), without taking into account turbulence terms and hydrodynamic pressure, as

$$\frac{\partial u}{\partial t} + \frac{\bar{u}_{-} u}{\Delta x} - \frac{\bar{u}_{-} u_{-1,}}{\Delta x} + \frac{\bar{w}_{-} u}{\Delta z} - \frac{\bar{w}_{-} u_{,-1}}{\Delta z} + g\frac{\partial \zeta}{\partial x} = 0 \quad \text{at } (i+1/2, k) \tag{19}$$

Multiplying Equation (16) by u and adding Equation (19) and then multiplying by $(\Delta x\ \Delta z)$, the momentum conservation equation for the control volume shown in Figure 1 is obtained

$$\Delta x \frac{\partial (u\Delta z)}{\partial t} + (\bar{u}_{+}\Delta z)u - (\bar{u}_{-}\Delta z)u_{-1,} + (\bar{w}_{+}\Delta x)u - (\bar{w}_{-}\Delta x)u_{,-1} + g\Delta z(\zeta_{+1/2} - \zeta_{-1/2}) = 0$$
$$\text{at } (i+1/2, k) \tag{20}$$

Similar approximations can be derived for the other flow directions (Appendix A).

It can be shown that Equation (17) integrated in the depth reduces to the one-dimensional approximation as described by Stelling *et al.* [4] when a uniform distribution of u in the vertical is assumed.

4.2. Momentum in the vertical direction

The continuity equation is discretized as Equation (16) and the momentum equation is approximated for positive flows as follows:

$$\frac{\partial w}{\partial t} + \bar{u}_{-}\left(\frac{w - w_{-1,}}{\Delta x}\right) + \bar{w}_{-}\left(\frac{w - w_{,-1}}{\Delta z}\right) = -\frac{\partial q}{\partial z} + \nu_{\mathrm{h}}\frac{\partial^2 w}{\partial x^2} + \frac{\partial}{\partial z}\left(\nu_{\mathrm{t}}\frac{\partial w}{\partial z}\right), \quad \text{at } (i, k+1/2) \tag{21}$$

where

$$\bar{w}_{+} = \frac{w_{i,k+1/2} + w_{i,k+3/2}}{2}$$

$$\bar{w}_{-} = \frac{w_{i,k-1/2} + w_{i,k+1/2}}{2}$$

$$\bar{u}_{+} = \frac{u_{i+1/2,k} + u_{i+1/2,k+1}}{2}$$

$$\bar{u}_{-} = \frac{u_{i-1/2,k} + u_{i-1/2,k+1}}{2} \tag{22}$$

$$w_{-1,} = w_{i-1,k}$$

$$w_{,-1} = w_{i,k-1/2}$$

The fact that Equation (21) describes a momentum balance can be demonstrated by rewriting Equation (21), without taking into account turbulence terms and hydrodynamic pressure, as

$$\frac{\partial w}{\partial t} + \frac{\bar{u}_{-} w}{\Delta x} - \frac{\bar{u}_{-} w_{-1,}}{\Delta x} + \frac{\bar{w}_{-} w}{\Delta z} - \frac{\bar{w}_{-} w_{,-1}}{\Delta z} = 0 \quad \text{at } (i, k+1/2) \tag{23}$$

Multiplying Equation (16) by w and adding Equation (23) and then multiplying by $(\Delta z \Delta x)$, the momentum conservation equation is obtained

$$\Delta z \frac{\partial (w \Delta x)}{\partial t} + (\bar{u}_{+} \Delta z) w - (\bar{u}_{-} \Delta z) w_{-1,} + (\bar{w}_{+} \Delta x) w - (\bar{w}_{-} \Delta x) w_{,-1} = 0 \quad \text{at } (i, k+1/2) \tag{24}$$

Similar approximations can be derived for the other flow directions (Appendix A).

5. TURBULENCE CLOSURE MODEL

The turbulence model implemented is the standard k–ε model [8]. The k–ε model either neglects the transport of individual turbulent stresses or accounts for them only in an approximate manner. In flow regions where the accurate description of this transport is important, for example, in regions where the eddy–viscosity concept breaks down, the transport equation for the individual stresses should be employed. However, many complex flows that do not satisfy the equilibrium hypothesis or the isotropic condition have been reproduced by the k–ε model with some modifications in the standard coefficients or in the equations, reporting substantial improvements. To model the near-wall region, damping functions are introduced to the k–ε model, resulting in the low-Reynolds number version of

this model. In the standard $k-\varepsilon$ model, the logarithmic law of the wall is applied; therefore a very fine mesh is not required.

5.1. The $k-\varepsilon$ model equations

Hereafter a short description of the governing equations is given. The two-equation turbulence closure for kinetic energy k and its dissipation ε reads

$$\frac{\partial \varepsilon}{\partial t}+\frac{\partial (u\varepsilon)}{\partial x}+\frac{\partial (w\varepsilon)}{\partial z}=\frac{\partial}{\partial x}\left[\frac{\nu_t}{\sigma_\varepsilon}\frac{\partial \varepsilon}{\partial x}\right]+\frac{\partial}{\partial z}\left[\frac{\nu_t}{\sigma_\varepsilon}\frac{\partial \varepsilon}{\partial z}\right]+\frac{\varepsilon}{k}\left[c_{1\varepsilon}P_k-c_{2\varepsilon}\varepsilon\right] \tag{25}$$

$$\frac{\partial k}{\partial t}+\frac{\partial (uk)}{\partial x}+\frac{\partial (wk)}{\partial z}=\frac{\partial}{\partial x}\left[\frac{\nu_t}{\sigma_k}\frac{\partial k}{\partial x}\right]+\frac{\partial}{\partial z}\left[\frac{\nu_t}{\sigma_k}\frac{\partial k}{\partial z}\right]+P_k-\varepsilon \tag{26}$$

where

$$P_k=-\overline{uu'}\frac{\partial u}{\partial x}-\overline{u'w'}\left[\frac{\partial u}{\partial z}+\frac{\partial w}{\partial x}\right]-\overline{w'w'}\frac{\partial w}{\partial z} \tag{27}$$

The terms representing the turbulent fluctuations are approximated by the Boussinesq hypothesis

$$\begin{aligned}
-\overline{u'u'}&=2\nu_t\frac{\partial u}{\partial x}\\
-\overline{w'w'}&=2\nu_t\frac{\partial w}{\partial z}\\
-\overline{u'w'}&=\nu_t\left[\frac{\partial u}{\partial z}+\frac{\partial w}{\partial x}\right]
\end{aligned} \tag{28}$$

where ν_t is the eddy viscosity, k is the turbulent kinetic energy and ε is the dissipation rate of the turbulent kinetic energy.

The eddy viscosity is related to k by

$$\nu_t=c_\mu\frac{k^2}{\varepsilon} \tag{29}$$

The empirical constants are given as $c_\mu=0.09$, $c_{1\varepsilon}=1.44$, $c_{2\varepsilon}=1.92$, $\sigma_k=1.0$ and $\sigma_\varepsilon=1.3$. The numerical implementation of the $k-\varepsilon$ model is described in detail by Stelling [9].

6. SIMULATION OF THE VERTICAL STRUCTURE OF HYDRAULIC JUMPS

The ability of the numerical method to simulate discontinuous flows is illustrated. Flow over a step where downstream a hydraulic jump forms is computed. Results from the numerical model are compared with experimental data from the literature [10,11]. This present case has particular characteristics that complicate its numerical modelling

- Discontinuities in the bottom profile.
- The hydrostatic assumption fails to reproduce the flow mainly because of the departure of the pressures from the hydrostatic values in the region downstream the step.
- The flow changes from sub-critical to supercritical (through the critical depth somewhere over the step) and then from supercritical to sub-critical (hydraulic jump).
- Two particular reversal flows should be represented, downstream of the structure (near the bed) and at the hydraulic jump surface (surface roller).

A channel length of $L = 3.5$ m is discretized with cells of equal size $\Delta x = \Delta z = 0.01$ m. At inflow, a depth-integrated velocity is prescribed of 0.083 $m^2 s^{-1}$ and at outflow a water depth (ht) of 0.155 m. The initial conditions are velocities equal zero and horizontal water levels. The calculation is carried out with a time step $\Delta t = 0.0025$ s and $\theta = 1.00$. After 5000 time steps the steady state is obtained. The number of vertical layers varies from six (minimum water depth) to 26 (maximum water depth).

Figure 3 shows the water levels and Figure 4 illustrates the velocity vectors. The water surface profile approaches to the measurements for $z_0 = 0.000025$ m.

Figure 5 depicts the horizontal velocities. Good agreement with the experiments is observed for all the profiles. An almost exact representation is obtained for reaches upstream of the structure and after the surface roller of the hydraulic jump ($x = 0.30$ m, 0.50 m and $x = 2.05$

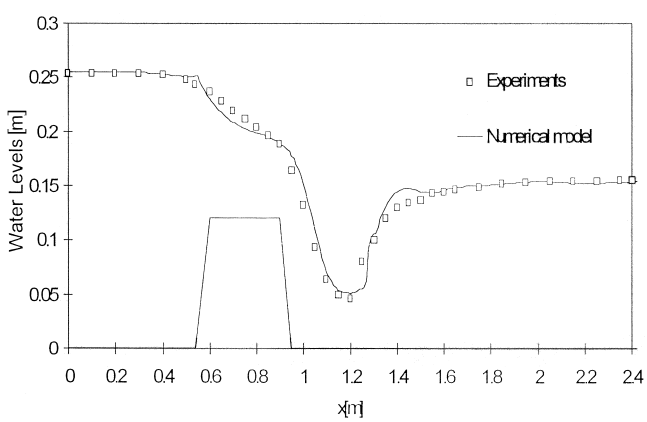

Figure 3. Comparison of water levels: □, experiments; —, numerical model.

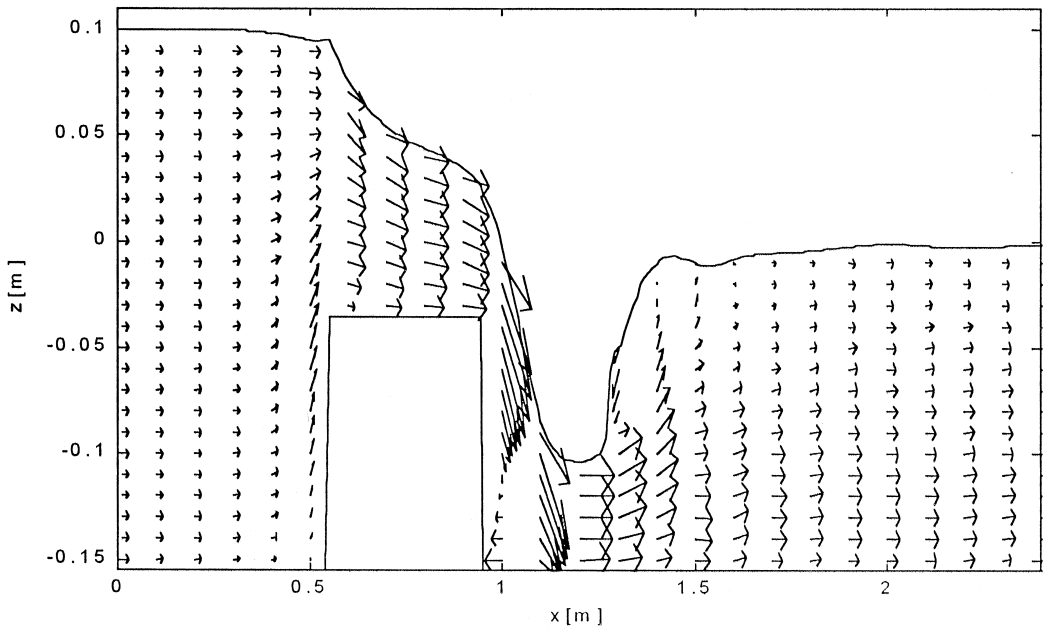

Figure 4. Velocity vectors obtained from the numerical model.

m, 2.40 m). Over the step, the measured velocities are more uniform than the predicted values ($x = 0.75$ m). Downstream of the structure ($x = 0.99$ m) the transition to reverse velocity in the vertical is linearly represented by the model from the height of the step to the bottom. However, in the experiments a very sharp change is observed to a certain height somewhat lower than the step; after that being almost uniform. Immediately after, the profiles obtained with the model approach the experimental values ($x = 1.07$ m). Then, in the supercritical reach, velocities near the bed are underpredicted ($x = 1.20$ m). In the transition to sub-critical flow, the surface roller velocities are well predicted; however, at the bottom the velocities are more uniform than the predicted values ($x = 1.26$ m and 1.85 m).

Figure 6 shows the vertical velocities. It can be seen that very good agreement with the experiments in all the reaches is achieved, except in the zone downstream of the structure ($x = 0.99$ m) where the reverse flow occurs near the bed and in the hydraulic jump where the surface roller is preponderant ($x = 1.35$ m).

In Figure 7 the Reynolds stresses are drawn. Again good agreement with the experiments is obtained, except for the zones in supercritical flow ($x = 1.20$ m) and in the length of the surface roller where they are underpredicted. After the surface roller, very good results are obtained ($x = 1.55$ m, 1.85 m, 2.05 m and 2.40 m).

Figure 8 depicts the variation of the average in the vertical Reynolds stresses along the reach. In Figure 9 the turbulence viscosity (ν_t) obtained from the numerical model is drawn in the vertical direction. This parameter shows the adaptation length of the transition from supercritical flow to the conditions where turbulence approaches to the corresponding values under uniform sub-critical flows.

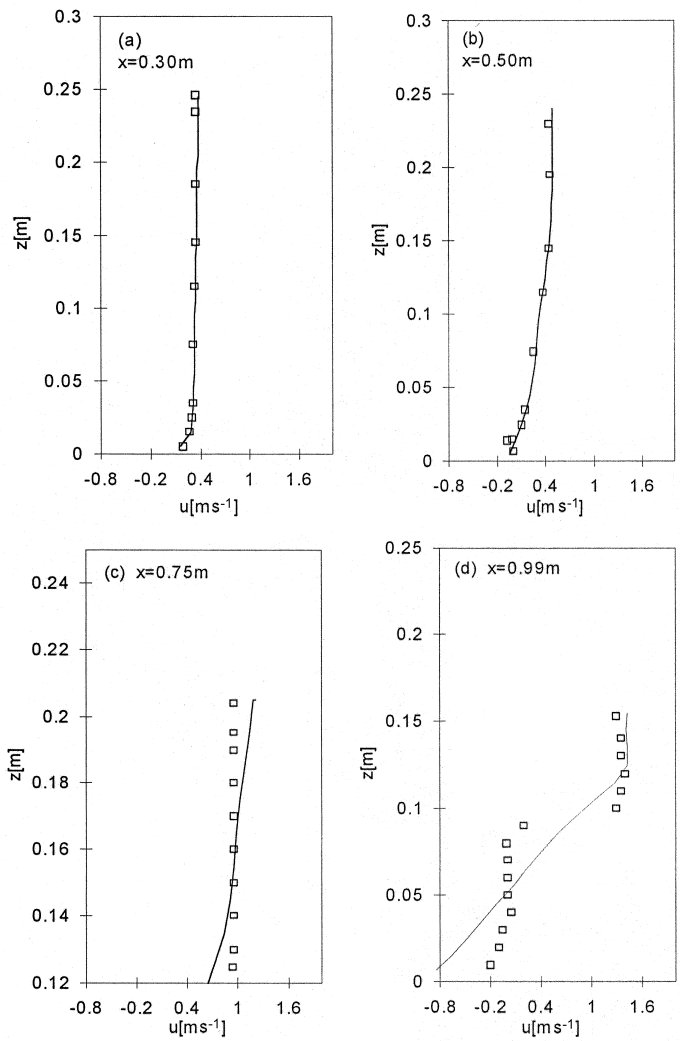

Figure 5. Comparison of horizontal velocity profiles: □, experiments; —, numerical model.

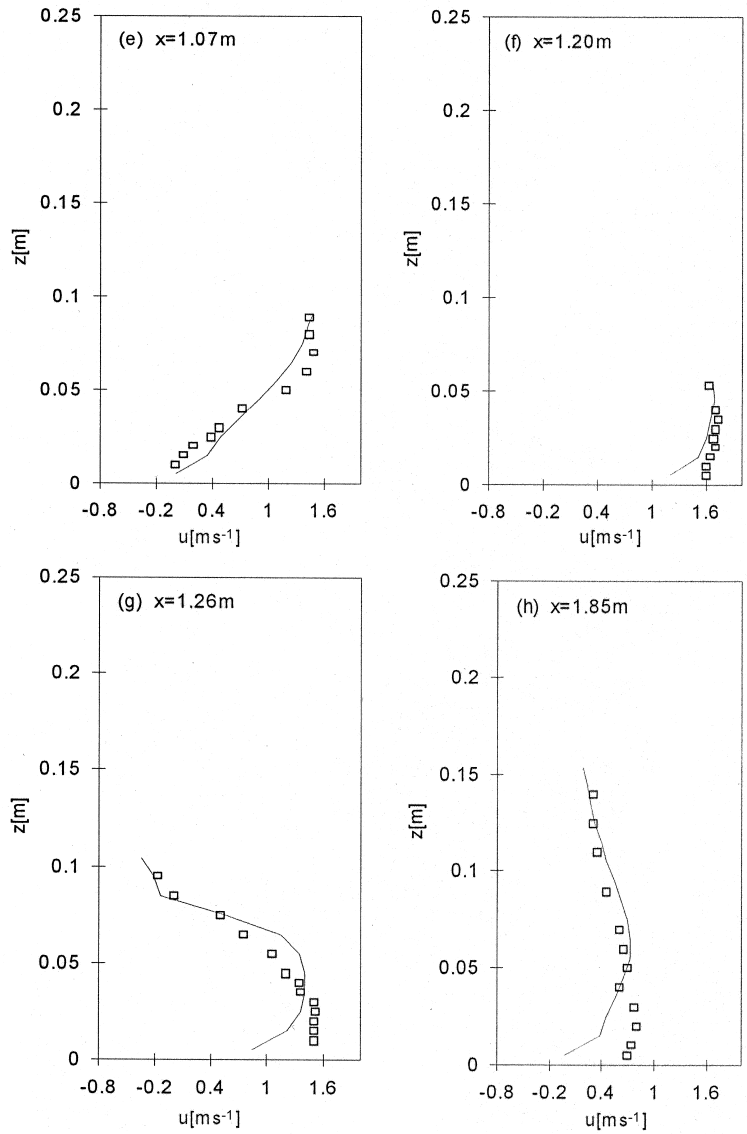

Figure 5 (*Continued*)

7. DISCUSSION OF THE RESULTS

The vertical structure of the flow was quite well reproduced, even though a coarse grid was defined. Major dispersion from the experimental data is found in the reverse flow, downstream

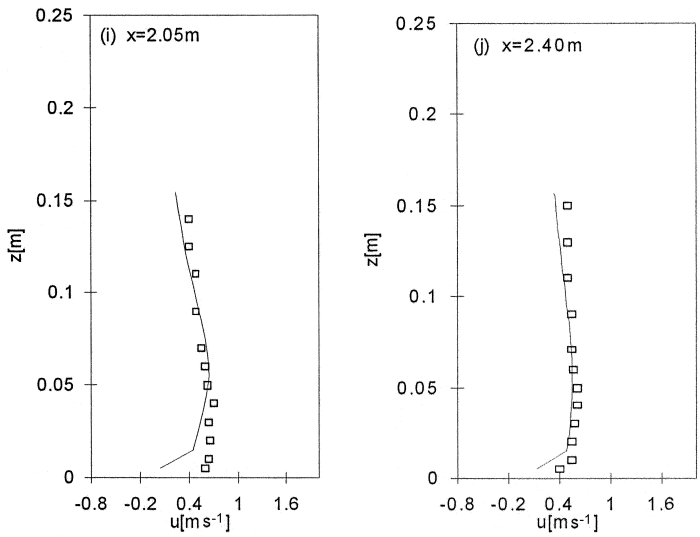

Figure 5 (*Continued*)

of the step and at the length of the hydraulic jump roller. At the supercritical reaches, horizontal velocities are underpredicted. The kind of errors observed are typical of the standard $k-\varepsilon$ turbulence closure model implemented.

The turbulence model could be further improved by applying a low-Reynolds number version of the $k-\varepsilon$ model, which will allow a better representation of velocities in the separation and reattachment points. These types of models have been shown to improve the predictions in the backward-facing step. However, when applied to the simulation of uniform supercritical flows, Prinos and Zeris [12] reported that the models fail to predict the reduction in the turbulence velocities u' with respect to sub-critical flows. The turbulence parameters in supercritical flows appear to be different from those in sub-critical flows, which have been extensively studied. Studies on supercritical flows are quite limited compared with sub-critical flows. Some turbulence studies are reported by Prinos and Zeris [12] and Tominaga and Nezu [13]. An anisotropic turbulence closure model appears more adequate to represent the supercritical flow and the transition to sub-critical flow along the length of the surface roller. Nevertheless, the length of this transition is well predicted by the numerical model.

8. CONCLUSIONS

A semi-implicit finite difference method for non-hydrostatic free-surface flows, in which advection terms in the momentum equations are approximated to fulfil a proper momentum

conservation, is proved to fairly accurately represent discontinuous flows. Its ability to simulate these flows is illustrated by computing the flow over a step where downstream of it a hydraulic jump is formed. This case has particular characteristics that restrict the application of existent numerical methods:

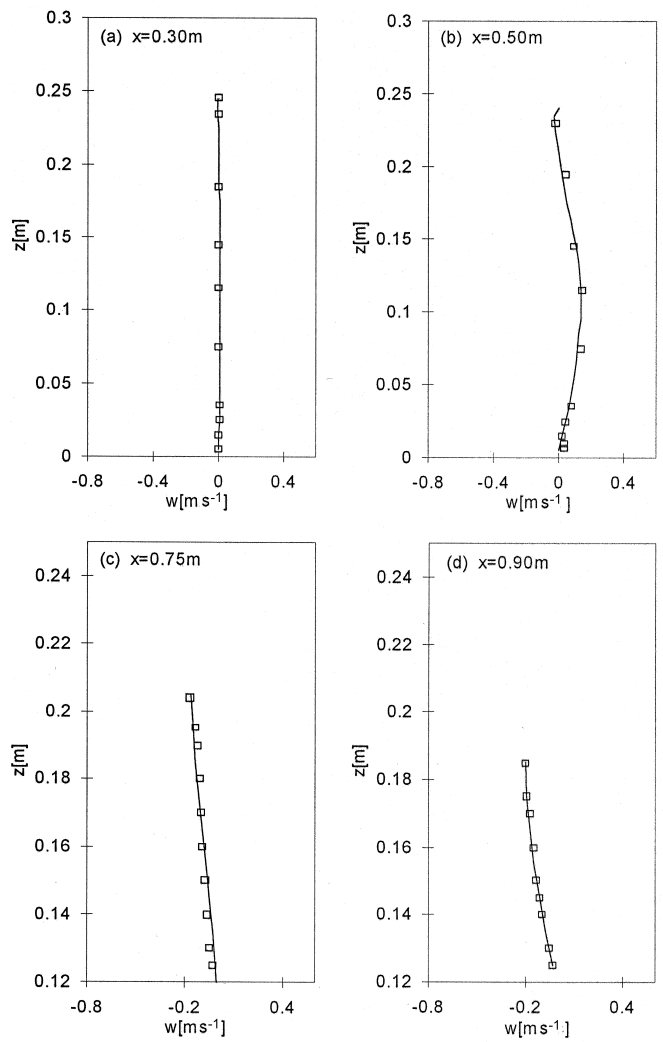

Figure 6. Comparison of vertical velocity profiles: □, experiments; —, numerical model.

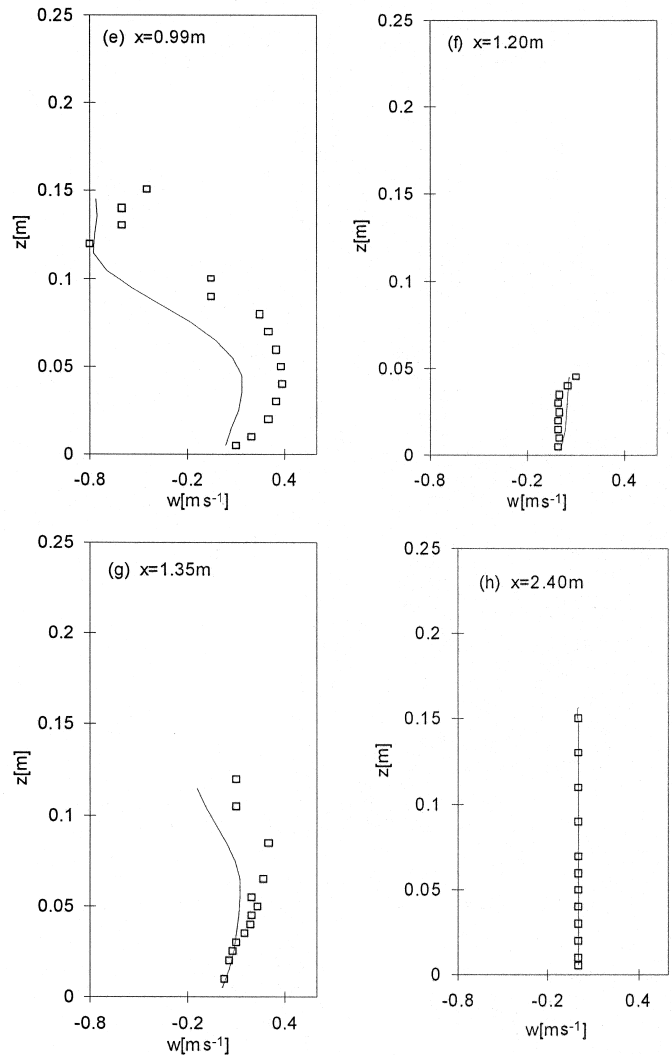

Figure 6 (*Continued*)

– abrupt changes of bottom topography;
– presence of mixed flows (sub-critical, critical and supercritical flows);
– the pressures downstream of the step highly deviate from the hydrostatic values;
– the hydraulic jump formation.

The results from the numerical model show good agreement with the experimental data. Deviation from the data is found in the reversal flow downstream of the step and at the length of the roller at the hydraulic jump. The errors observed are found to be inherent to the standard $k-\varepsilon$ turbulence closure model implemented.

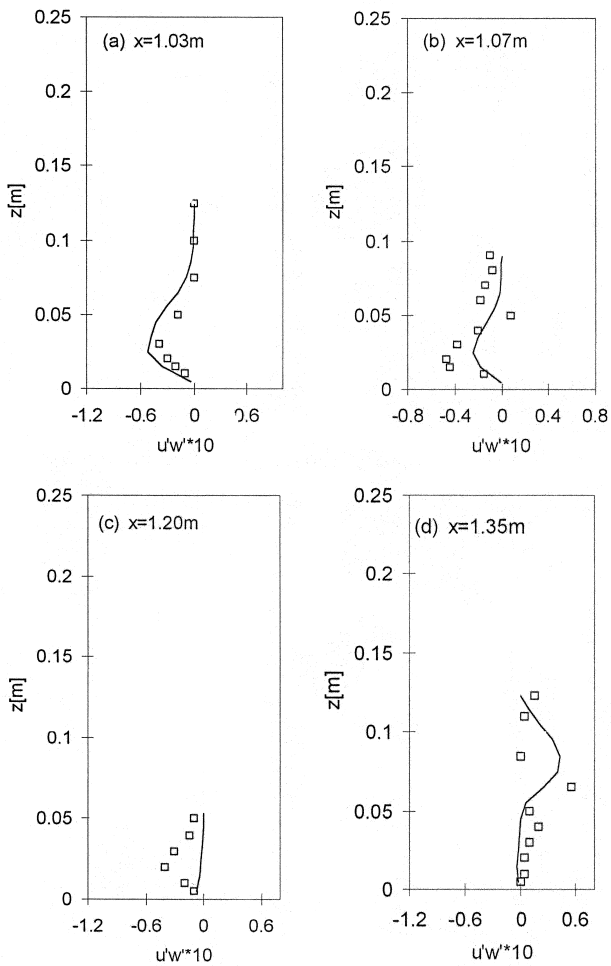

Figure 7. Comparison of Reynolds stresses: □, experiments; —, numerical model.

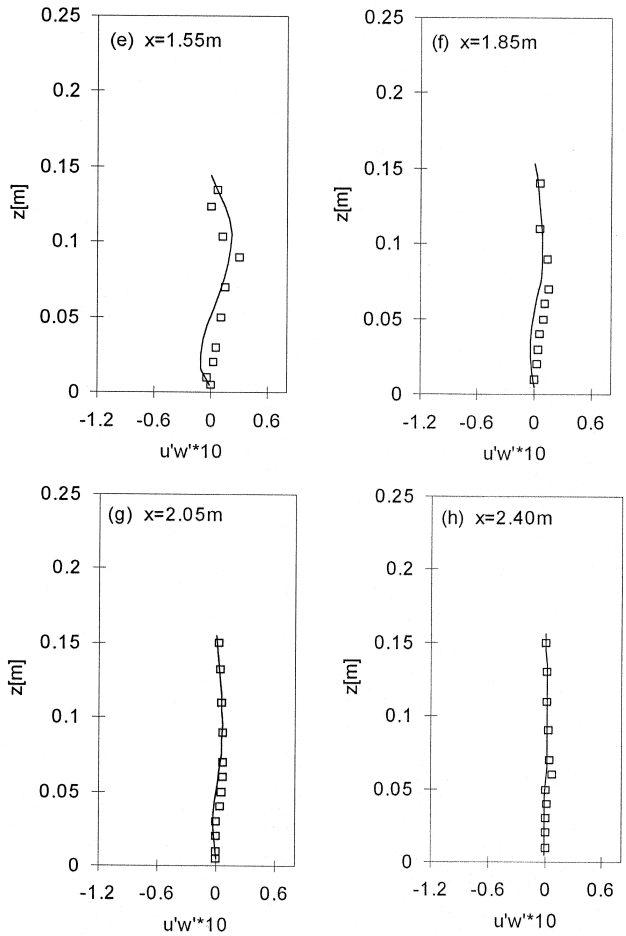

Figure 7 (*Continued*)

This numerical model is shown to be a useful tool in the design of structures. The length of the bed protection downstream of a hydraulic jump could be predicted based on the hydraulic jump position for a pre-design structure and on the adaptation length of the hydraulic jump. Furthermore, the model could be used as a flow module towards the morphological modelling of discontinuous flows where the representation of the vertical structure becomes relevant as in the case of local scour assessment.

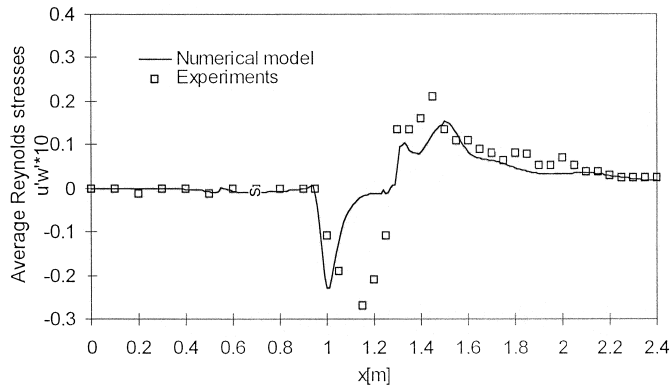

Figure 8. Comparison of average Reynolds stresses: □, experiments; —, numerical model.

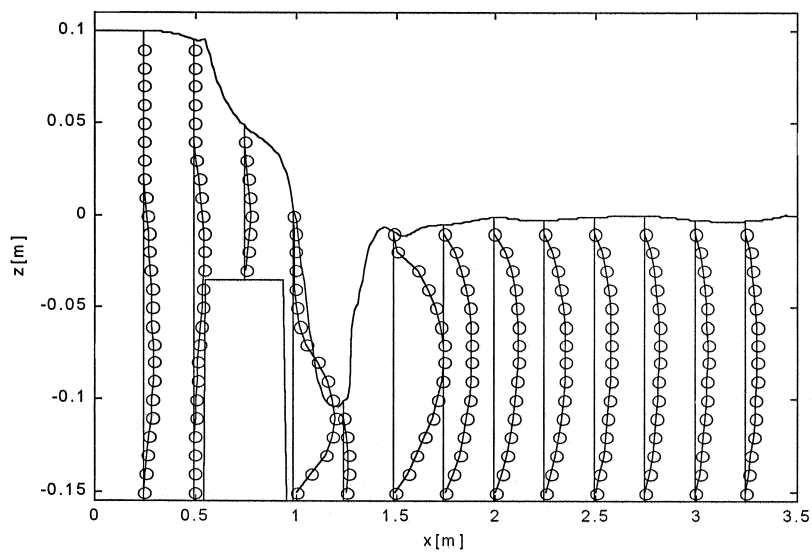

Figure 9. Turbulence viscosity obtained from the numerical model.

APPENDIX A. ADVECTION TERMS

A.1. Advection terms momentum in the x-direction

Horizontal advection

The advection terms for the different flow directions are

$$\begin{aligned}
&\bar{u}_+ > 0 \cap \bar{u}_- > 0, \qquad \bar{u}_-\left(\frac{u - u_{-1,}}{\Delta x}\right)\\
&\bar{u}_+ < 0 \cap \bar{u}_- < 0, \qquad \bar{u}_+\left(\frac{u_{+1,} - u}{\Delta x}\right)\\
&\bar{u}_+ < 0 \cap \bar{u}_- > 0, \qquad \bar{u}_+\left(\frac{u_{+1,} - u}{\Delta x}\right) + \bar{u}_-\left(\frac{u - u_{-1,}}{\Delta x}\right)
\end{aligned} \tag{A1}$$

Vertical advection

The advection terms for the different flow directions are

$$\begin{aligned}
&\bar{w}_+ > 0 \cap \bar{w}_- > 0, \qquad \bar{w}_-\left(\frac{u - u_{,-1}}{\Delta z}\right)\\
&\bar{w}_+ < 0 \cap \bar{w}_- < 0, \qquad \bar{w}_+\left(\frac{u_{,+1} - u}{\Delta z}\right)\\
&\bar{w}_+ < 0 \cap \bar{w}_- > 0, \qquad \bar{w}_+\left(\frac{u_{,+1} - u}{\Delta z}\right) + \bar{w}_-\left(\frac{u - u_{,-1}}{\Delta z}\right)
\end{aligned} \tag{A2}$$

A.2. Advection terms momentum in the z-direction

Horizontal advection

The advection terms for the different flow directions are

$$\begin{aligned}
&\bar{u}_+ > 0 \cap \bar{u}_- > 0, \qquad \bar{u}_-\left(\frac{w - w_{-1,}}{\Delta x}\right)\\
&\bar{u}_+ < 0 \cap \bar{u}_- < 0, \qquad \bar{u}_+\left(\frac{w_{+1,} - w}{\Delta x}\right)\\
&\bar{u}_+ < 0 \cap \bar{u}_- > 0, \qquad \bar{u}_+\left(\frac{w_{+1,} - w}{\Delta x}\right) + \bar{u}_-\left(\frac{w - w_{-1,}}{\Delta x}\right)
\end{aligned} \tag{A3}$$

Vertical advection

The advection terms for the different flow directions are

$$\begin{aligned}
&\bar{w}_+ > 0 \cap \bar{w}_- > 0, \qquad \bar{w}_-\left(\frac{w - w_{,-1}}{\Delta z}\right)\\
&\bar{w}_+ < 0 \cap \bar{w}_- < 0, \qquad \bar{w}_+\left(\frac{w_{,+1} - w}{\Delta z}\right)\\
&\bar{w}_+ < 0 \cap \bar{w}_- > 0, \qquad \bar{w}_+\left(\frac{w_{,+1} - w}{\Delta z}\right) + \bar{w}_-\left(\frac{w - w_{,-1}}{\Delta z}\right)
\end{aligned} \tag{A4}$$

REFERENCES

1. Chaudhry MH. *Open-channel Flow*. Prentice-Hall: New York, 1993.
2. Alcrudo F, García-Navarro P. A high-resolution Godunov-type scheme in finite volumes for the 2D shallow water equations. *International Journal for Numerical Methods in Fluids* 1993; **16**: 489–505.
3. Toro EF. *Riemann Solvers and Numerical Methods for Fluids Dynamics*. Springer: Berlin, 1997.
4. Stelling GS, Kernkamp HWJ, Laguzzi MM. Delft flooding system: a powerful tool for inundation assessment based upon a positive flow simulation. In *Proceedings of the 3rd International Conference on Hydroinformatics*, Copenhagen, Denmark, Babovic A, Larsen A (eds). A.A. Balkema Publishers: Rotterdam, 1998; 449–456.
5. Leendertse JJ. Aspects of a computational model for long period water-wave propagation. RAND Corporation Memorandum RM-5294-PR, 1967.
6. Casulli V. Semi-implicit finite difference methods for two-dimensional shallow water equations. *Journal of Computational Physics* 1990; **86**: 56–74.
7. Casulli V, Stelling GS. Numerical simulation of three-dimensional quasi-hydrostaitc, free-surface flows. *Journal of Hydraulic Engineering ASCE* 1998; **124**(7): 678–686.
8. Rodi W. Turbulence models and their applications in hydraulics. State of the Art Paper, IAHR, 1980.
9. Stelling GS. Compact differencing for stratified free surface flow. In *Advances in Hydro-Science and -Engineering*. Edited and Published by the Chinese Hydraulic Engineering Society, vol. II. Beijing, China, 1995; 378–386.
10. González EM. Estudio experimental de flujos disipativos: Resalto hidraulico. MSc thesis, Esc. tecn. sup. de ing. de caminos, canales y puertos. Dep. de Ciencias y Tecnicas del agua y del medio ambiente. Universidad de Cantabria, Santander, Spain (in Spanish), 1992.
11. González EM, Losada MA. *Estudio experimental de un resalto hidraulico*. Ciencia y Tecnica de la Ingeniería Civil. Revista de obras públicas 3.330, Año 141, Marzo, 1994; 47–65 (in Spanish).
12. Prinos P, Zeris A. Uniform flow in open channels with steep slopes. *Journal of Hydraulic Research* 1996; **33**(5): 705–719.
13. Tominaga A, Nezu I. Velocity profiles in steep open channel flows. *Journal of Hydraulic Engineering ASCE* 1992; **118**(1): 73–90.

